New Journal of Physics

The open access journal at the forefront of physics

CrossMark

PAPER

Multiple Auger cycle photoionisation of manganese atoms by short soft x-ray pulses

S Klumpp[1,2], N Gerken[2], K Mertens[2], M Richter[3], B Sonntag[2], A A Sorokin[1,4], M Braune[1,5], K Tiedtke[1], P Zimmermann[6] and M Martins[2]

1 FS-FLASH-D, Deutsches Elektronen-Synchrotron (DESY), Notkestraße 85, D-22607 Hamburg, Germany
2 Department Physik, Universität Hamburg, Luruper Chaussee 149, D-22761 Hamburg, Germany
3 Physikalisch-Technische Bundesanstalt (PTB), Abbestraße 2-12, D-10587 Berlin, Germany
4 Ioffe Physico-Technical Institute, Polytekhnicheskaya 26, 194021 St. Petersburg, Russia
5 FS-FLASH-O, Deutsches Elektronen-Synchrotron (DESY), Notkestraße 85, D-22607 Hamburg, Germany
6 Institut für Optik und Atomare Physik, TU Berlin, Hardenbergstraße 36, D-10623 Berlin, Germany

E-mail: stephan.klumpp@desy.de

Keywords: nonlinear photoionisation, short x-ray pulses, atomic open shell system

Abstract

The multiple ionisation of atomic Mn, excited at (photon energy: 52.1 eV) and above (photon energy: 61.1 eV) the discrete giant $3p$–$3d$ resonance, was studied using high irradiation free-electron-laser soft x-ray pulses from the BL2 beamline of FLASH, DESY, Hamburg. In particular, the impact of the giant resonance on the ionisation mechanism was investigated. Ion mass-over-charge spectra were obtained by means of ion time-of-flight spectrometry. For the two photon energies, the yield of the different ionic charge states Mn^{q+} ($q = 0$–7) was determined as a function of the irradiance of the soft x-ray pulses. The maximum charge state observed was Mn^{6+} for resonant excitation at 52.1 eV and Mn^{7+} for non-resonant excitation at 61.1 eV at a maximum irradiation of 3×10^{13} Wcm^{-2}.

1. Introduction

Since the discovery of the photoelectric effect by Hertz [1] and its explanation by Einstein [2] it has been used extensively to study the interaction between light and matter. In the standard quantum mechanical formulation, one photon interacts with one electron of a given atomic shell. With the upcoming lasers in the 1960s, the ionisation of atoms with optical light via multi-photon absorption became possible [3] using an optical ruby laser with a wavelength of 694.3 nm (photon energy: 1.78 eV). The nonlinear multi-photon photoionisation was afterwards an active field in the 1970s and 1980s [4–8], but limited to the optical regime because only optical lasers were able to generate sufficiently high electromagnetic fields [9, 10]. The vacuum ultra-violet (VUV) regime between 10 and 200 nm (photon energy: 6–124 eV) was reached 12 years ago [11–15] using higher harmonic generation schemes (see e.g. [7, 16]) while the first light source generating pulses in the soft x-ray regime with sufficient photon densities [17] for multi-photon excitation was the free electron laser (FEL) FLASH (formerly TTF [18]) built by DESY [19–21]. Using short pulses of about 100 fs pulse length at 13 eV photon energy and peak irradiances of the order of 1×10^{13} W cm^{-2}, the multiple outer shell ionisation of rare gases was demonstrated [22, 23]. Later, the work of multi-photon ionisation on rare gases was extended up to 39 eV photon energy [24–26]. At the VUV-FEL facility SCSS in Japan, the multi-photon multiple ionisation of argon was reported at 20 eV and 2×10^{14} W cm^{-2} [27].

First inner shell excitation using soft x-ray FEL pulses with a duration in the order of a few tenths of femtoseconds was reported for a photon energy of 90 eV and irradiance up to 1×10^{16} W cm^{-2} on Xe [28]. A charge state up to Xe^{21+} was reached which requires in total more than 57 photons to be absorbed within the duration of the single pulse. Later, at the x-ray FEL facility LCLS, the complete stripping of the ten electrons of Ne [29] and charge states up to 36+ on Xe [30] were observed at photon energies in the keV regime explained by cycles of core excitations with subsequent Auger decay and resonance enhanced photoabsorption.
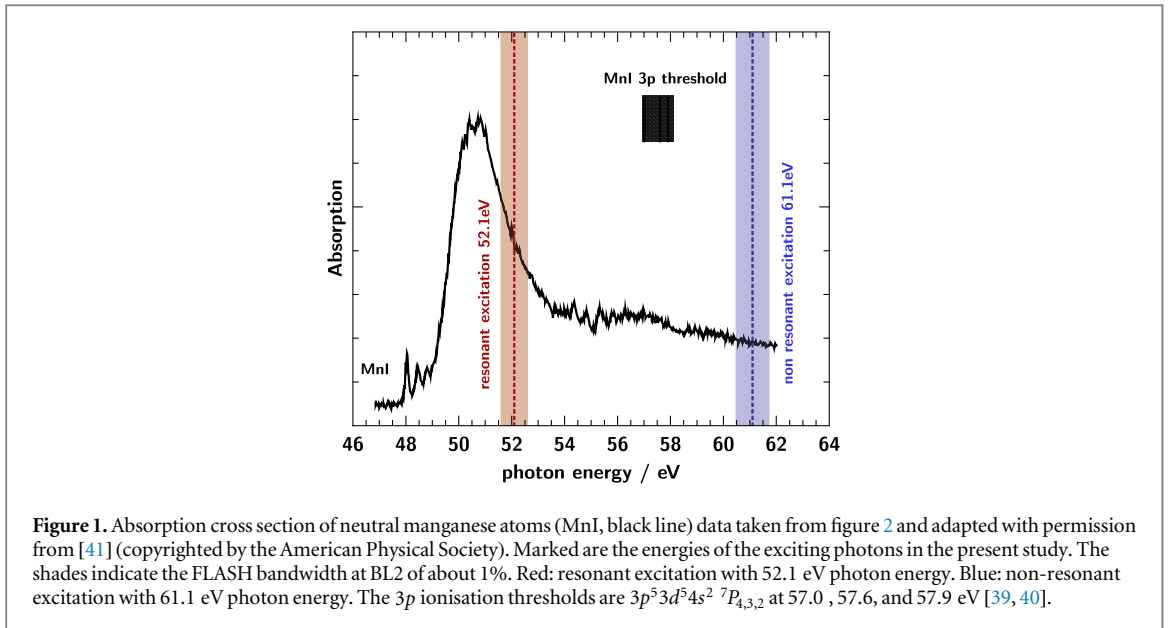
Figure 1. Absorption cross section of neutral manganese atoms (MnI, black line) data taken from figure 2 and adapted with permission from [41] (copyrighted by the American Physical Society). Marked are the energies of the exciting photons in the present study. The shades indicate the FLASH bandwidth at BL2 of about 1%. Red: resonant excitation with 52.1 eV photon energy. Blue: non-resonant excitation with 61.1 eV photon energy. The $3p$ ionisation thresholds are $3p^5 3d^5 4s^2$ $^7P_{4,3,2}$ at 57.0 , 57.6, and 57.9 eV [39, 40].
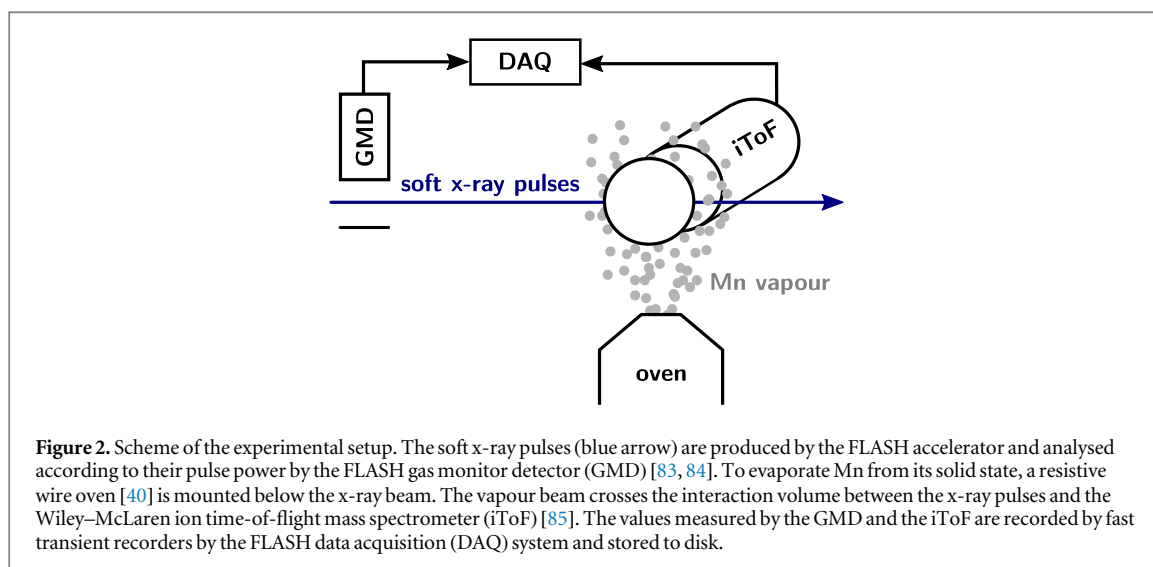
The physics driving the high degree of ionisation of Xe in the soft x-ray regime is, however, still under debate [31–33]. Especially, the 'giant' resonance caused by the transition from $4d$ to εf around 90 eV is considered to enhance the absorption of many photons in contrast to the lighter noble gases [34, 35] where no such resonance exists. Using photoelectron spectroscopy it was proven that two x-ray photons can indeed be absorbed simultaneously in the 'giant' resonance of Xe [36, 37]. Moreover it has been shown that the ionising behaviour of Xe strongly depends on the pulse duration [38]. The latter work demonstrates the different mechanisms of multi-photon excitation and ionisation including sequential processes via decaying resonances.

Similar to Xe, the spectrum of Mn atoms displays a giant resonance in the VUV regime spanning the photon energy range 49–53 eV [39, 40]. In contrast to the Xe $4d-\varepsilon f$ continuum giant resonance located above the $4d$ ionisation threshold, the $3p-3d$ resonance of the open shell Mn atoms is discrete, i.e. it lies below the $3p$ ionisation thresholds. The $3p$ absorption spectrum and the $3p$ ionisation thresholds of neutral manganese are shown in figure 1.

The $3p-3d$ resonance was studied in the past using absorption spectroscopy for neutral manganese [41, 42] as well as for Mn^{1+} to Mn^{3+} [41, 43–49]. In case of the singly charged Mn^{1+} ion the absolute value of the cross section has been determined [50]. The electronic multiplet structure of Mn, on the other hand, was studied using photoelectron spectroscopy [39, 51–58]. Various theoretical concepts were developed to describe the cross section behaviour of the $3p-3d$ transition: generalised Fano theory [59–63], ('spin-polarised') random phase approximation with exchange (SP)PRAE [64–73], Compton scattering [74], and the Breit–Pauli R-matrix formalism [75, 76], as well as potential barrier effects like in Xe [77]. Comprehensive reviews can be found in [40, 78]. Since the $3d$ shell of neutral Mn and the Mn ions is partially filled, many $3p^5 3d^{n+1}$ states are accessible after the $3p$ excitation [41]. They are strongly coupled to the $3p^6 3d^{n-1} \varepsilon (p/f)$ super Coster–Kronig continua [41, 79, 80] decaying within sub femtoseconds [81]. Thus, high photon intensities allow for fast excitation into high ionic charge states via $3p-3d$ excitation/de-excitation cycles until all $3d$ electrons are removed. In any case, as has been shown for Xe, (giant) resonances can significantly enhance the multi-photon ionisation of atomic systems at high irradiance. Since the resonances in Xe and Mn are of very different character, as mentioned above, the goal of the present study is to clarify the contribution of a discrete giant resonance, i.e. the Mn $3p-3d$ resonance, to multi-photon multiple ionisation. For this purpose, metal vapours of open-shell Mn atoms were investigated at high evaporation temperature.

2. Methods

For the preparation of an effusive atomic beam, Mn was evaporated under vacuum conditions. The base pressure of our experimental chamber was in the order of 5×10^{-9} hPa to minimise residual gas. To achieve a partial pressure of Mn atoms of the order of 1×10^{-3}–1×10^{-2} hPa in the interaction region, required for the experiments, a temperature in the oven between 1100 and 1300 K had to be applied [82] which was achieved by using a resistive wire oven [40]. The aperture of the crucible had a diameter of 5 mm producing an effusive beam of manganese vapour. The vapour was crossed with the pulsed focused photon beam from FLASH in the

Figure 2. Scheme of the experimental setup. The soft x-ray pulses (blue arrow) are produced by the FLASH accelerator and analysed according to their pulse power by the FLASH gas monitor detector (GMD) [83, 84]. To evaporate Mn from its solid state, a resistive wire oven [40] is mounted below the x-ray beam. The vapour beam crosses the interaction volume between the x-ray pulses and the Wiley–McLaren ion time-of-flight mass spectrometer (iToF) [85]. The values measured by the GMD and the iToF are recorded by fast transient recorders by the FLASH data acquisition (DAQ) system and stored to disk.

interaction region of the mass-spectrometer (figure 2). The temperature of the oven was strictly controlled to keep the chamber pressure lower than 5×10^{-7} hPa during the measurements. For the excitation of the Mn atoms, soft x-ray pulses from the beamline BL2 at FLASH were used. The beamline delivers photon pulses with a typical energy bandwidth of one percent of the photon energy [20, 86] and a pulse duration in the order of $\tau = (100 \pm 10)$ fs (FWHM). The latter was estimated by measuring a single-shot spectral intensity profile at the PG2 beamline of FLASH before and after the experiment as well as by online determination of the length of the electron bunch [87]. Two different photon energies were chosen. Photons of 52.1 eV photon energy excite the Mn atoms within the giant $3p$–$3d$ resonance whereas of 61.1 eV photon energy can ionise the $3p$ shell (see figure 1) [41, 43, 44]. These photon energies and the corresponding bandwidths are marked in figure 1.
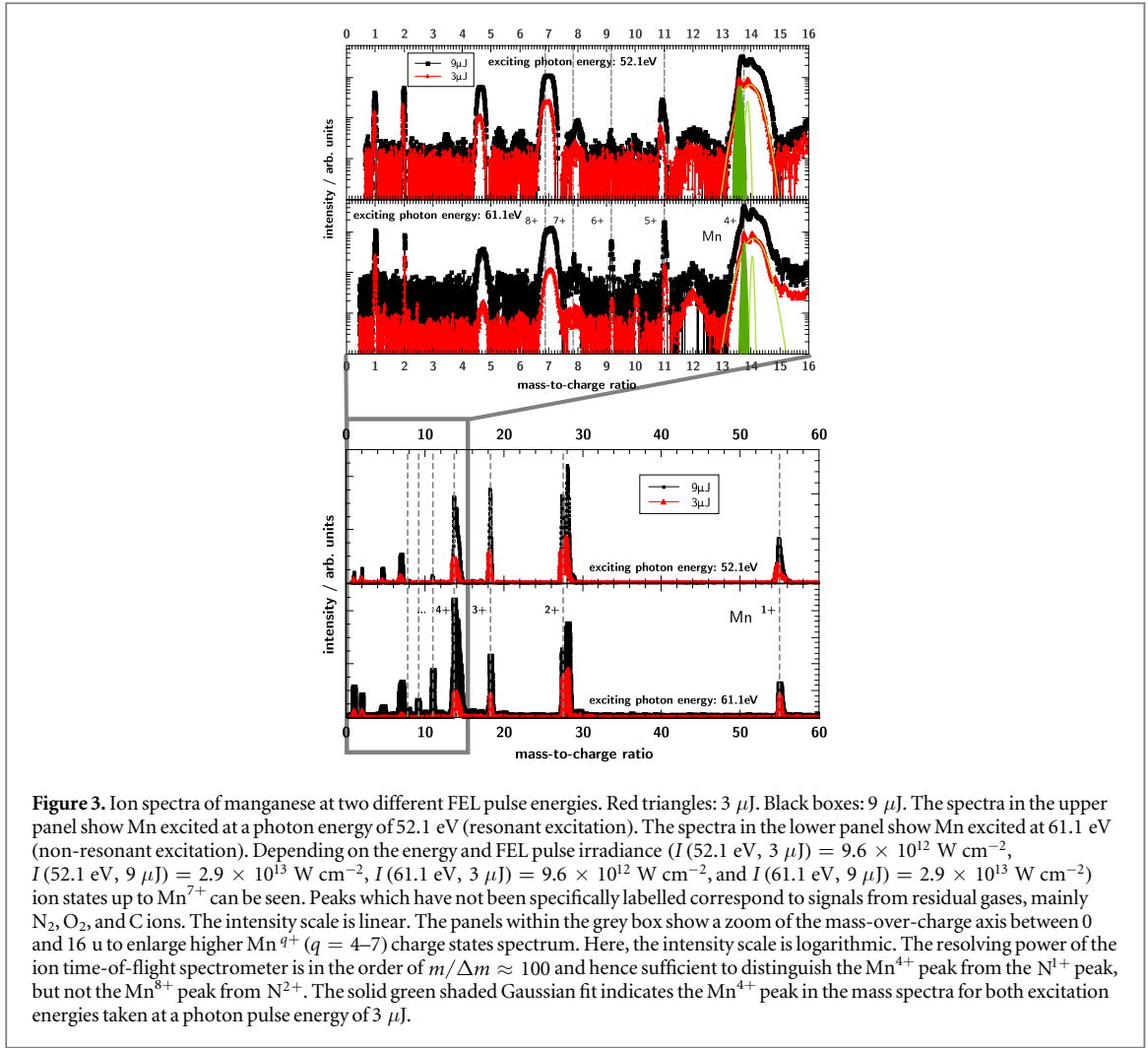
The radiation was distributed among 10 pulse trains per second. Each train was filled with 80 pulses separated by 4 μs [20, 84, 86]. The photon beam was focused by the BL2 ellipsoidal mirror [84] down to (20 ± 5) μm in the diameter (FWHM) with Rayleigh length of about 13 mm. The focused beam characteristics were determined using the atomic gas photoionisation techniques [88], a method based an ablation of solids [89], and with the help of a wave front sensor [90–92]. Due to the self-amplified spontaneous emission process in the FLASH accelerator, the photon pulse energy varies statistically and significantly from shot to shot [20, 93]. This enabled us to study the ionisation scaling with pulse energy of Mn atoms in the range from 1 to 9 μJ while keeping the focal spot area constant from shot to shot. The pulse energy for each single pulse was measured on-line in a non-destructive way using the gas monitor detector (GMD) installed in front of the first optical element of the FLASH beamline [83, 84]. The absolute GMD pulse energies could be determined with an uncertainty of about 10%.

For Mn ions, created upon photoionisation of the neutral Mn atoms, the mass-over-charge ratio was determined by a Wiley–McLaren-type time-of-flight spectrometer (iToF) [85, 94]. It was equipped with a V-stack of MCPs and had an acceptance length along the photon beam of 10 mm.

Separately for the two different photon energies, the raw spectra were sorted according to the energy of the FLASH pulse determined by the GMD. All spectra lying within an energy interval of 0.6 μJ for resonant excitation and 0.25 μJ for non-resonant excitation around the the selected energy were summed (binned). Two different energy intervals for the binning were chosen because both measurements were performed at two different days during the beamtime and hence the FEL operation was not the same for both. The energy intervals chosen guaranteed comparable statistics for both plots. In order to correct for the varying vapour density and the different number of spectra summed up for one bin, these spectra were normalised to the total number of ions detected and the number of spectra per bin.

3. Results

Plotting the ion intensity versus the mass-to-charge ratio after the binning process, ion spectra as shown in figure 3 were obtained. The upper panels depict spectra excited with a photon energy of 52.1 eV, the lower panels depict spectra excited with a photon energy of 61.1 eV. In each panel, the spectra with red triangles are excited with FEL pulses of 3 μJ pulse energy and the one with black boxes are excited with pulses of 9 μJ. The irradiance I

Figure 3. Ion spectra of manganese at two different FEL pulse energies. Red triangles: 3 μJ. Black boxes: 9 μJ. The spectra in the upper panel show Mn excited at a photon energy of 52.1 eV (resonant excitation). The spectra in the lower panel show Mn excited at 61.1 eV (non-resonant excitation). Depending on the energy and FEL pulse irradiance (I (52.1 eV, 3 μJ) $= 9.6 \times 10^{12}$ W cm^{-2}, I (52.1 eV, 9 μJ) $= 2.9 \times 10^{13}$ W cm^{-2}, I (61.1 eV, 3 μJ) $= 9.6 \times 10^{12}$ W cm^{-2}, and I (61.1 eV, 9 μJ) $= 2.9 \times 10^{13}$ W cm^{-2}) ion states up to Mn^{7+} can be seen. Peaks which have not been specifically labelled correspond to signals from residual gases, mainly N$_2$, O$_2$, and C ions. The intensity scale is linear. The panels within the grey box show a zoom of the mass-over-charge axis between 0 and 16 u to enlarge higher Mn $^{q+}$ (q = 4–7) charge states spectrum. Here, the intensity scale is logarithmic. The resolving power of the ion time-of-flight spectrometer is in the order of $m/\Delta m \approx$ 100 and hence sufficient to distinguish the Mn^{4+} peak from the N^{1+} peak, but not the Mn^{8+} peak from N^{2+}. The solid green shaded Gaussian fit indicates the Mn^{4+} peak in the mass spectra for both excitation energies taken at a photon pulse energy of 3 μJ.

of the pulses, which represents a key quantity of the radiation field to describe multi-photon processes, was calculated according to [28]:

$$I = \frac{W}{A \cdot \tau},$$ (1)

where W is the FEL pulse energy, A is the focal spot area, and τ is the pulse duration. For the four spectra in figure 3, one obtains I (52.1 eV, 3 μJ) $= 9.6 \times 10^{12}$ W cm^{-2}, I (52.1 eV, 9 μJ) $= 2.9 \times 10^{13}$ W cm^{-2}, I (61.1 eV, 3 μJ) $= 9.6 \times 10^{12}$ W cm^{-2}, and I (61.1 eV, 9 μJ) $= 2.9 \times 10^{13}$ W cm^{-2}. The absolute value of the irradiance has an uncertainty of 30%. The main contributions to this uncertainty are due to the difficulties encountered in the exact determination of the focal spot area A and the pulse length τ. The error bars, however, for the irradiance axis given in figure 4 reflect the shot-to-shot variation of the pulse energy measured by the GMD of 10%. The position of the different charged ionic states are marked by grey dashed lines. During the experiment we were able to measure ions from Mn^{1+} up to Mn^{7+} depending on the irradiance and on the exciting photon energy. The intensity of an ion species was determined by integrating the area beneath a respective ionic peak by fitting the peak with one or multiple Gaussian functions depending on overlapping residual gas peaks nearby. The uncertainty of the results is smaller for isolated than for overlapping peaks. For the worst case, the Mn^{4+} peak at 13.75 u overlapping the N^{1+} peak at 14 u, the numerical uncertainty rises to a maximum of 20%. The different statistics for each bin, as discussed above, adds a maximum uncertainty of 3%. This uncertainty is based on the fact that a minimum of 1000 spectra have been summed for each bin. A further uncertainty is caused by the correction for the varying density of the Mn vapour in the interaction volume, as described above. The total uncertainty for the ion yield, given by the error bars in figure 4, was obtained by an propagation of uncertainty calculation taking all above uncertainties for the ion yield into account. Plotting the determined values over the irradiance, one gets plots as presented in figure 4. The ion yields for 52.1 eV photon excitation are plotted in the upper panel (a) of figure 4, the ion yields for 61.1 eV photon excitation are plotted in the lower panel (b), respectively. Same colours and symbols in figure 4 mark the same ionic state of Mn $^{q+}$ (q = 1–7). Note that the ion yield is given in logarithmic scale. The spectra for the different ions, over most of the

Figure 4. Ion yield of different Mn^{q+} ($q = 1$–7) charge states depending on the irradiance of the FEL pulses of FLASH. Upper panel (a): excitation of the Mn ionic charge states with photons of 52.1 eV. Lower panel (b): excitation of the Mn ionic charge states with photons of 61.1 eV. Dotted lines: fit of the data point with equation (3). The curves were fitted by using the Levenberg–Marquardt algorithm [95, 96] in its representation in the GNU Scientific Library [97].

irradiance range covered, can be approximated by a straight line, corresponding to the power law introduced by [98, 99] for the description of the multi-photon process:

$$\frac{N_q}{N} \sim I^n, \tag{2}$$

where N_q is the ion yield of the charge state q, N the number of atomic targets, I the irradiance , and n the number of photons needed to reach the charge state q. By normalising the data to the sum of all Mn^{q+} yields which should be dominated by single photon processes ($n \approx 1$), one obtains:

$$\log\left(\frac{N_q}{\sum_q N_q}\right) \sim (n - 1) \tag{3}$$

i.e., the number of photons n needed to populate a certain Mn^{q+} ion can be determined by fitting the slope $k \approx n - 1$ on a logarithmic scale. Single photon excitation ($n \approx 1$) results, hence, in a constant line with $k = 0$. For high irradiance, however, lower charged ions like Mn^{1+} get depleted resulting in a negative slope in figure 4. Here, equation 3 is not valid any more, but still useful as it indicates this saturation effect. The results are listed in table 1. For both photon energies, the k values for the charge states up to $q = 4$ are smaller than 1 or even negative indicating the depletion of the ionic species. In contrast to this, the curves for Mn charge states $q = 5$ to $q = 7$ excited by 61.1 eV display a markedly steeper slope with k values in the order of 2 for Mn^{5+}, Mn^{6+}, and larger than 3 for Mn^{7+}. For 52.1 eV photon energy, only the k value for Mn^{6+} exceeds 1. For Mn^{1+} to Mn^{4+}, for both photon energies, the ion yields drop with increasing charge state but all yields lie within an order of magnitude. This significantly changes for the step from Mn^{4+} to Mn^{5+}. At low irradiance, the yield for Mn^{5+} is more than an order of magnitude lower than that of Mn^{4+}. For 52.1 eV the difference is almost constant, at all irradiance values, whereas for 61.1 eV the Mn^{5+} yield is only by approximately a factor of 2 lower than the Mn^{4+}

Table 1. Values for the slopes k obtained by fitting the curves in figure 4 by equation (3) using the Levenberg–Marquardt algorithm [95, 96] in its representation in the GNU Scientific Library [97]. The numerical error of all values is in the order of 0.3. For the discussion of the values refer to the text.

Ionic state $q+$	Slope k for	
	52.1 eV photon excitation	61.1 eV photon excitation
Mn^{1+}	-0.25	-0.3
Mn^{2+}	0.03	-0.1
Mn^{3+}	0.2	0.4
Mn^{4+}	0.4	0.6
Mn^{5+}	0.5	1.7
Mn^{6+}	1.3	2.2
Mn^{7+}		3.5

Table 2. Electron configurations and ionisation energies of the Mn^{q+} ($q = 0$–7) ground charged states according to *NIST Atomic Spectra Database* [100]. The given multi-step ionisation energy is needed to excite the respective ionic state from the neutral ground state. The number of photons given are needed to excite the next ionic state. For example, to reach the highest ionic state Mn^{7+} by sequential ionisation from the neutral ground state in total 11 photons of 52.1 eV or 10 photons of 61.1 eV are required. For the direct multi-photon Mn to Mn^{7+} ionisation 8 respectively 7 photons would do.

(Ionic) Atomic ground state configuration		Single-step Ionisation energy	Multi-step	No. of photons needed per step	
				For 52.1 eV	For 61.1 eV
Mn	$3p^6 3d^5 4s^2 (^6S_{5/2})$	7.43 eV	7.43 eV	1	1
Mn^{1+}	$3p^6 3d^5 4s (^7S_3)$	15.64 eV	23.07 eV	1	1
Mn^{2+}	$3p^6 3d^5 (^6S_{5/2})$	33.67 eV	56.74 eV	1	1
Mn^{3+}	$3p^6 3d^4 (^5D_0)$	51.20 eV	107.94 eV	1	1
Mn^{4+}	$3p^6 3d^3 (^4F_{3/2})$	72.40 eV	180.34 eV	2	2
Mn^{5+}	$3p^6 3d^2 (^3F_2)$	95.60 eV	275.94 eV	2	2
Mn^{6+}	$3p^6 3d (^2D_{3/2})$	119.20 eV	395.14 eV	3	2
Mn^{7+}	$3p^6 (^1S_0)$	195.50 eV	590.64 eV		

yield at the highest irradiance. This is reflected by the significantly different k values. For 52.1 eV the k values for Mn^{4+} and Mn^{5+} are almost the same, whereas for 61.1 eV the k value increases from 0.6 for Mn^{4+} to 1.7 for Mn^{5+}. For 52.1 eV, the Mn^{5+} yield, over the whole irradiance range, can be well approximated by a straight line. This is not the case for 61.1 eV, where the slope decreases markedly for higher irradiance. For both photon energies, the yield drops from Mn^{5+} to Mn^{6+} by an order of magnitude. This also holds for the step from Mn^{6+} to Mn^{7+} which could only be generated by 61.1 eV photons at an irradiance above 1×10^{13} W cm^{-2}.

4. Discussion

The above results make it clear that the n values cannot simply be related to the number of photons involved in the excitation like for a two level system. The reason for this rests with the sequential ionisation process by which ion states up to $q = 4$ are generated. A low n value indicates that the corresponding ionisation step is close to saturation.

Table 2 gives the electron configurations and the ionisation energies of the Mn^{q+} ($q = 0$–7) ground states [100]. Successively stripping the $4s$ and $3d$ valence electrons ionic states up to Mn^{4+} can be reached by single-photon ionisation. For the generation of Mn^{5+}, Mn^{6+}, and Mn^{7+} more than one photon is required for each ionisation step. However, for photon energies close to the $3p$ threshold, the direct $4s$ ionisation is negligible [101]. For 52.1 eV, within the giant $3p$–$3d$ resonance, discrete $3p^6 3d^5 4s^2 \rightarrow 3p^5 3d^6 4s^2$ excitation followed by the ultrafast super Coster–Kronig decay to $3p^6 3d^4 4s^2 \varepsilon\ell$ dominates the ionisation step. At 61.1 eV, above the $3p$ ionisation threshold, direct $3d$ ionisation and to a lesser extent $3p$ ionisation give rise to the first step. At this energy, the cross section σ_{3d} is approximately four times larger than the cross section σ_{3p} [52]. The $3p$ hole will dominantly decay via super Coster–Kronig decay to $3p^6 3d^3 4s^2$.
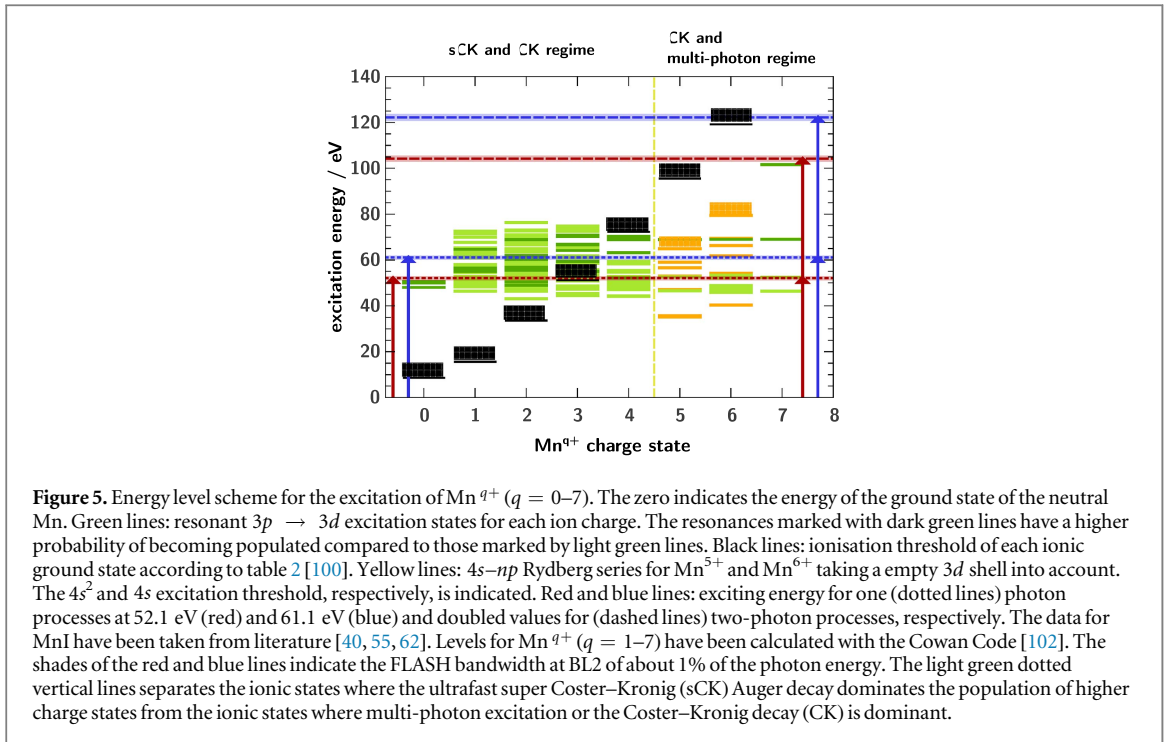
Figure 5. Energy level scheme for the excitation of Mn^{q+} ($q = 0$–7). The zero indicates the energy of the ground state of the neutral Mn. Green lines: resonant $3p \rightarrow 3d$ excitation states for each ion charge. The resonances marked with dark green lines have a higher probability of becoming populated compared to those marked by light green lines. Black lines: ionisation threshold of each ionic ground state according to table 2 [100]. Yellow lines: $4s$–np Rydberg series for Mn^{5+} and Mn^{6+} taking a empty $3d$ shell into account. The $4s^2$ and $4s$ excitation threshold, respectively, is indicated. Red and blue lines: exciting energy for one (dotted lines) photon processes at 52.1 eV (red) and 61.1 eV (blue) and doubled values for (dashed lines) two-photon processes, respectively. The data for MnI have been taken from literature [40, 55, 62]. Levels for Mn^{q+} ($q = 1$–7) have been calculated with the Cowan Code [102]. The shades of the red and blue lines indicate the FLASH bandwidth at BL2 of about 1% of the photon energy. The light green dotted vertical lines separates the ionic states where the ultrafast super Coster–Kronig (sCK) Auger decay dominates the population of higher charge states from the ionic states where multi-photon excitation or the Coster–Kronig decay (CK) is dominant.

In order to gain insight into the processes involved reaching higher charge states up to Mn^{4+} with single photon absorption, we performed calculations with the Cowan Code [102] calculating the resonances of the different Mn^{q+} ($q = 1$–7) ionic states. Especially, the photon-energy needed to excite the $3p \rightarrow 3d$ transition in the Mn^{q+} ($q = 1$–7) ions and to create the $3p^{-1}$ hole for a subsequent super-Coster–Kronig Auger decay is calculated. The results are shown in figure 5 as an excitation energy scheme. The levels of the neutral Mn atom are taken from literature [40, 55, 62]. The green lines in figure 5 indicate possible $3p$–$3d$ excitation resonances obtained with the Cowan Code [102]. The dark green lines are considered to be strong resonances having a weighted oscillator strength of $gf > 0.1$ as obtained directly from the Cowan Code, the light green ones have weighted oscillator strengths of $gf < 0.1$. A short explanation of gf can be found in [103]. The ground state configurations from which the $3d$ electrons are removed via a $3p$–$3d$ excitation and a subsequent super Coster–Kronig Auger decay are MnII $3p^6 3d^4 4s^2$ ^5D, MnIII $3p^6 3d^3 4s^2$ ^4F, MnIV $3p^6 3d^2 4s^2$ ^3F, MnV $3p^6 3d 4s^2$ ^2D, MnVI $3p^6 \, 4s^2$ ^1S, MnVII $3p^6 \, 4s$ ^2S and MnVIII $3p^6$ $^1S_0$. The yellow lines for Mn^{5+} and Mn^{6+} are the $4s$–np Rydberg series for the configuration Mn^{5+} $3p^6 4s^2$ and Mn^{6+} $3p^6 4s$, respectively, indicating the ionisation threshold needed to excite a valence $4s$ electron into the continuum when the $3d$ shell is empty. The value for Mn^{5+} $3p^6 4s^2$ is (65 ± 1) eV and for Mn^{6+} $3p^6 4s$ it is (79 ± 1) eV.

The black levels indicate the first ionisation threshold in respect to each ionic ground state according to table 2 [100]. The red and blue lines indicate the exciting photon energy. The lower ones mark the one-photon threshold for the resonant excitation energy at 52.1 eV (red) and non-resonant excitation energy at 61.1 eV (blue). The upper ones mark the two-photon threshold at twice the photon energy, respectively.

Figure 5 shows that the $3p^6 \, 3d^n \, 4s^2$–$3p^5 \, 3d^{n+1} \, 4s^2$ ($n = 1$–4) resonances largely cover the range of the two exciting photon energies. The $3p^5 \, 3d^{n+1} \, 4s^2$ core resonances are strongly coupled to the $3p^6 \, 3d^{n-1} \, 4s^2 \, \varepsilon\ell$ ionisation continua as has been shown for neutral Mn, which results in a considerable broadening and energy shift of the resonances. The discrete resonances merge into the giant $3p$–$3d$ resonance shown in figure 1 and one may expect similar effects for the Mn^{q+} $3p^5 \, 3d^n \, 4s^2$ ($q = 1$–3, $n = 2$–4) ions. In addition to the super Coster–Kronig decay $3p^5 \, 3d^{n+1} \, 4s^2$–$3p^6 \, 3d^{n-1} \, 4s^2 \, \varepsilon\ell$, also the Coster–Kronig decay $3p^5 \, 3d^{n+1} \, 4s^2$–$3p^6 \, 3d^n \, 4s \, \varepsilon\ell$ contributes to the decay of the $3p^{-1}$ core hole. This is consistent with the ionisation threshold for $3d^n \, 4s^2$–$3d^{n-1} \, 4s^2 \, \varepsilon\ell$ of 46.2 eV for Mn^{2+} and for $3d^n \, 4s^2$–$3d^n \, 4s \, \varepsilon\ell$ of 37.4 eV calculated in single configuration calculations with the Cowan Code [102]. Full fledged calculations of the complex level structure, the transition probabilities and the decay rates, taking the many electron interaction into account, are very demanding and have only been performed for neutral Mn (see i.e. review [40, 78]).

In spite of the above caveats, it is well justified to describe the observed generation of the ions Mn^{q+} ($q = 1$–3) mainly to the sequential $3p$–$3d$ photoexcitation followed by the ultrafast super Coster–Kronig decay. For the step from Mn^{3+} to Mn^{4+} the weaker Coster–Kronig decay of the $3p$–$3d$ resonance has to be invoked. The interpretation of the results by this resonant $3p$–$3d$ excitation ultrafast Auger decay cycle is consistent with

the ion yields for the Mn^{q+} ($q = 1$–4). Via this cycle mainly the Mn^{4+} $3p^6$ $3d$ $4s^2$ and $3p^6$ $3d^2$ $4s$ configurations are populated.

At 52.1 eV exciting photon energy, the slope k of the Mn^{5+} yield is almost the same as the slope for the Mn^{4+} yield (see figure 4 and table 1), but the ion yield for Mn^{5+} drops by almost an order of magnitude. One photon is not sufficient anymore to excite Mn^{4+} into an excited state which has enough energy to autoionise, because for the ionisation from Mn^{4+} to Mn^{5+} 72.4 eV are needed (see table 2 [100]) which exceeds the energy of our chosen photon energies. Mn^{5+} can only be reached via a two-photon process which causes the drop in the ion yield. Excitations of the $3p^6$ $3d^1$ $4s^2$ $\rightarrow$ $3p^5$ $3d^2$ $4s^2$ or $3p^6$ $3d^2$ $4s$ $\rightarrow$ $3p^5$ $3d^3$ $4s$ resonances predicted close to 52.1 eV probably dominate the first step. For Mn^{6+} only a few data points could be determined, precluding any interpretation.

For 61.1 eV photon excitation energy, there is no corresponding $3p$–$3d$ resonance. Therefore the step from Mn^{4+} to Mn^{5+} is driven by single photon $4s$ ionisation or a two-photon $3d$ ionisation. The same processes will also contribute to the step from Mn^{5+} to Mn^{6+}. The step from Mn^{6+} to Mn^{7+} can only proceed via multi-photon $4s$ ionisation requiring 79.5 eV. This tentative interpretation is consistent with the experimental k values (see table 1) rising from 1.7 for Mn^{5+} to 2.2 for Mn^{6+} and 3.5 for Mn^{7+}. The drop of the ion yield by a factor of 10 for each of those steps supports these conclusions. To reach even higher charge states within the single FEL pulse, the remaining $3d$ and $4s$ electrons have to be removed from the respective ion until the process stops at Mn^{6+} and Mn^{7+} for the photon energy of 52.1 eV and 61.1 eV, respectively. The production of ions with charge states higher than Mn^{7+} requires the excitation of the, now, valence $3p$ electrons and the respective photon energy of at least 195.5 eV (see table 2 [100]). In the present experiment, this excitation energy can be reached by three-photon processes only. Charge states above Mn^{7+} have, however, not been observed. Because the Mn^{8+} peak is buried under the strong residual gas N^{2+} peak and all higher Mn charge states are too weak at the irradiance level reached.

5. Conclusion

To summarise, we have studied the ionisation behaviour of Mn after excitation with intense soft x-ray pulses from the FEL FLASH in Hamburg at photon energies of 52.1eV and 61.1 eV and irradiances between 3×10^{12} W cm^{-2} and 3×10^{13} W cm^{-2}. Up to Mn^{4+}, cycles of (giant) discrete $3p$–$3d$ excitations followed by (super) Coster–Kronig decays can be regarded as the main ionisation routes close to saturation. For higher charges, more than one photon per step is involved. The behaviour is in analogy to Xe between 90 eV and 100 eV photon energy where the generation of charge states up to 5+ is dominated by cycles of (giant) continuum $4d$–εf excitations followed by Auger decay [38] and multiphoton steps up to 8+. The generation of even higher Mn charges by giant collective excitation/ionisation processes as discussed for Xe is scheduled for future investigations at even higher irradiances.

Acknowledgments

References

[1] Hertz H 1887 *Ann. Phys., Lpz.* **267** 983–1000
[2] Einstein A 1905 *Ann. Phys., Lpz.* **322** 132–48
[3] Voronov G and Delone N 1965 *JETP* **1** 66
[4] Lambropoulos P 1976 Topics on multiphoton processes in atoms *Advances in Atomic and Molecular Physics* (vol 12) ed D Bates and B Bederson (New York: Academic) pp 87–164
[5] Lambropoulos P and Tang X 1987 *J. Opt. Soc. Am.* B **4** 821–32
[6] Mainfray G and Manus G 1991 *Rep. Prog. Phys.* **54** 1333
[7] Protopapas M, Keitel C H and Knight P L 1997 *Rep. Prog. Phys.* **60** 389
[8] Delone N and Krainov V 2000 *Multiphoton Process in Atoms* (New York: Springer)
[9] Yamakawa K, Aoyama M, Matsuoka S, Kase T, Akahane Y and Takuma H 1998 *Opt. Lett.* **23** 1468–70

[10] Yamakawa K, Akahane Y, Fukuda Y, Aoyama M, Inoue N, Ueda H and Utsumi T 2004 *Phys. Rev. Lett.* **92** 123001

[11] ISO 21348 2007, *Space environment (natural and artificial) - Process for determining solar irradiances*, International Organization for Standardization

[12] Miyamoto N, Kamei M, Yoshitomi D, Kanai T, Sekikawa T, Nakajima T and Watanabe S 2004 *Phys. Rev. Lett.* **93** 083903

[13] Nabekawa Y, Hasegawa H, Takahashi E J and Midorikawa K 2005 *Phys. Rev. Lett.* **94** 043001

[14] Hasegawa H, Takahashi E J, Nabekawa Y, Ishikawa K L and Midorikawa K 2005 *Phys. Rev. A* **71** 023407

[15] Benis E P, Charalambidis D, Kitsopoulos T N, Tsakiris G D and Tzallas P 2006 *Phys. Rev. A* **74** 051402

[16] Salières P, L'Huillier A, Antoine P and Lewenstein M 1999 Study of the spatial and temporal coherence of high-order harmonics *Advances in Atomic, Molecular, and Optical Physics* ed B Bederson and H Walther vol 41 (New York: Academic) pp 83–142

[17] Ayvazyan V *et al* 2002 *Phys. Rev. Lett.* **88** 104802

[18] Schneider J R 2010 *J. Phys. B: At. Mol. Opt. Phys.* **43** 194001

[19] Ayvazyan V *et al* 2006 *Eur. Phys. J. D* **37** 297–303

[20] Ackermann W *et al* 2007 *Nat. Photon.* **1** 336–42

[21] Feldhaus J 2010 *J. Phys. B: At. Mol. Opt. Phys.* **43** 194002

[22] Wabnitz H, de Castro A R B, Gürtler P, Laarmann T, Laasch W, Schulz J and Möller T 2005 *Phys. Rev. Lett.* **94** 023001

[23] Laarmann T, de Castro A R B, Gürtler P, Laasch W, Schulz J, Wabnitz H and Möller T 2005 *Phys. Rev. A* **72** 023409

[24] Nagasono M *et al* 2007 *Phys. Rev. A* **75** 051406

[25] Sorokin A A, Wellhöfer M, Bobashev S V, Tiedtke K and Richter M 2007 *Phys. Rev. A* **75** 051402

[26] Moshammer R *et al* 2007 *Phys. Rev. Lett.* **98** 203001

[27] Motomura K *et al* 2009 *J. Phys. B: At. Mol. Opt. Phys.* **42** 221003

[28] Sorokin A A, Bobashev S V, Feigl T, Tiedtke K, Wabnitz H and Richter M 2007 *Phys. Rev. Lett.* **99** 213002

[29] Young L *et al* 2010 *Nature* **466** 56–61

[30] Rudek B *et al* 2012 *Nat. Photon.* **6** 858

[31] Makris M G, Lambropoulos P and Mihelic A 2009 *Phys. Rev. Lett.* **102** 033002

[32] Lambropoulos P, Papamihail K G and Decleva P 2011 *J. Phys. B: At. Mol. Opt. Phys.* **44** 175402

[33] Richter M 2011 *J. Phys. B: At. Mol. Opt. Phys.* **44** 075601

[34] Richter M, Amusia M Y, Bobashev S V, Feigl T, Juranic P N, Martins M, Sorokin A A and Tiedtke K 2009 *Phys. Rev. Lett.* **102** 163002

[35] Richter M, Bobashev S V, Sorokin A A and Tiedtke K 2010 *J. Phys. B: At. Mol. Opt. Phys.* **43** 194005

[36] Richardson V *et al* 2010 *Phys. Rev. Lett.* **105** 013001

[37] Mazza T *et al* 2015 *Nat. Commun.* **6** 6799

[38] Gerken N, Klumpp S, Sorokin A, Tiedtke K, Richter M, Bürk V, Mertens K, Juranic P and Martins M 2014 *Phys. Rev. Lett.* **112** 213002

[39] Malutzki R, Banna M S, Braun W and Schmidt V 1985 *J. Phys. B: At. Mol. Phys.* **18** 1735

[40] Sonntag B and Zimmermann P 1992 *Rep. Prog. Phys.* **55** 911

[41] Costello J T, Kennedy E T, Sonntag B F and Clark C W 1991 *Phys. Rev. A* **43** 1441–50

[42] Bruhn R, Sonntag B and Wolff H 1978 *Phys. Lett. A* **69** 9–11

[43] Cooper J W, Clark C W, Cromer C L, Lucatorto T B, Sonntag B F and Tomkins F S 1987 *Phys. Rev. A* **35** 3970–3

[44] Cooper J W, Clark C W, Cromer C R, Lucatorto T B, Sonntag B F, Kennedy E T and Costello J T 1989 *Phys. Rev. A* **39** 6074–7

[45] Donnelly D, Bell K L and Hibbert A 1996 *Phys. Rev. A* **54** 974–6

[46] Kilbane D, Kennedy E T, Mosnier J P, van Kampen P and Costello J T 2005 *J. Phys. B: At. Mol. Opt. Phys.* **38** L1

[47] Kilbane D, Mayo R, van Kampen P, Mosnier J P, Kennedy E T and Costello J T 2007 *Phys. Rev. A* **75** 062503

[48] Osawa T, Obara S, Nagata T, Azuma Y and Koike F 2009 *J. Phys. B: At. Mol. Opt. Phys.* **42** 085005

[49] Osawa T, Kawajiri K, Suzuki N, Nagata T, Azuma Y and Koike F 2012 *J. Phys. B: At. Mol. Opt. Phys.* **45** 225204

[50] Kjeldsen H, Folkmann F, Kristensen B, West J B and Hansen J E 2004 *J. Phys. B: At. Mol. Opt. Phys.* **37** 1321

[51] Krause M O, Carlson T A and Fahlman A 1984 *Phys. Rev. A* **30** 1316–24

[52] Jimenez-Mier J, Krause M O, Gerard P, Hermsmeier B and Fadley C S 1989 *Phys. Rev. A* **40** 3712–20

[53] Whitfield S B, Krause M O, van der Meulen P and Caldwell C D 1994 *Phys. Rev. A* **50** 1269–86

[54] Whitfield S B, Wehlitz R and Martins M 2004 *Radiat. Phys. Chem.* **70** 3–42

[55] Meyer M, Prescher T, Raven E, Richter M, Schmidt E, Sonntag B and Wetzel H E 1986 *Z. Phys. D* **2** 347–62

[56] Ford M J, Pejcev V, Smith D, Ross K J and Wilson M 1990 *J. Phys. B: At. Mol. Opt. Phys.* **23** 4247

[57] von dem Borne A *et al* 2000 *Phys. Rev. A* **62** 052703

[58] Penttilä A, Heinäsmäki S, Harkoma M, Fritzsche S, Sankari R, Aksela S and Aksela H 2005 *Phys. Rev. A* **71** 022715

[59] Davis L and Feldkamp L 1976 *Solid State Commun.* **19** 413–6

[60] Davis L C and Feldkamp L A 1977 *Phys. Rev. B* **15** 2961–9

[61] Dehmer J L, Starace A F, Fano U, Sugar J and Cooper J W 1971 *Phys. Rev. Lett.* **26** 1521–5

[62] Davis L C and Feldkamp L A 1978 *Phys. Rev. A* **17** 2012–22

[63] Davis L C and Feldkamp L A 1981 *Phys. Rev. B* **23** 6239–53

[64] Amusia M Y and Dolmatov V K 1993 *J. Phys. B: At. Mol. Opt. Phys.* **26** 1425

[65] Dolmatov V 1993 *Phys. Lett. A* **174** 116–8

[66] Dolmatov V K 1993 *J. Phys. B: At. Mol. Opt. Phys.* **26** L79

[67] Dolmatov V K and Amusia M Y 1994 *J. Phys. B: At. Mol. Opt. Phys.* **27** L281

[68] Dolmatov V K 1996 *J. Phys. B: At. Mol. Opt. Phys.* **29** L687

[69] Dolmatov V K and Mansurov M M 1996 *J. Phys. B: At. Mol. Opt. Phys.* **29** L307

[70] Dolmatov V K and Manson S T 1998 *J. Phys. B: At. Mol. Opt. Phys.* **31** 999

[71] Dolmatov V K and Manson S T 2006 *Phys. Rev. A* **74** 032705

[72] Dolmatov V K and Manson S T 2007 *Phys. Rev. A* **75** 022701

[73] Dolmatov V K, Kheifets A S, Deshmukh P C and Manson S T 2015 *Phys. Rev. A* **91** 053415

[74] Hopersky A N, Nadolinsky A M, Novikov S A and Yavna V A 2013 *J. Phys. B: At. Mol. Opt. Phys.* **46** 155202

[75] Donnelly D, Bell K L and Hibbert A 1997 *J. Phys. B: At. Mol. Opt. Phys.* **30** L285

[76] Donnelly D, Bell K L and Hibbert A 1998 *J. Phys. B: At. Mol. Opt. Phys.* **31** L971

[77] Frolov M V, Manakov N L and Starace A F 2010 *Phys. Rev. A* **82** 023424

[78] Martins M, Godehusen K, Richter T, Wernet P and Zimmermann P 2006 *J. Phys. B: At. Mol. Opt. Phys.* **39** R79

[79] Fano U 1961 *Phys. Rev.* **124** 1866–78

[80] Fano U and Cooper J 1965 *Phys. Rev.* **137** A1364–79

[81] Coster D and Kronig R D L 1935 *Physica* **2** 13–24
[82] Desai P D 1987 *J. Phys. Chem. Ref. Data* **16** 91–108
[83] Tiedtke K *et al* 2008 *J. Appl. Phys.* **103** 094511
[84] Tiedtke K *et al* 2009 *New J. Phys.* **11** 023029
[85] Wiley W C and McLaren I H 1955 *Rev. Sci. Instrum.* **26** 1150–7
[86] Feldhaus J, Arthur J and Hastings J B 2005 *J. Phys. B: At. Mol. Opt. Phys.* **38** S799
[87] Düsterer S *et al* 2014 *Phys. Rev. Accelerators Beams* **17** 120702
[88] Sorokin A A *et al* 2006 *Appl. Phys. Lett.* **89** 221114
[89] Chalupsky J *et al* 2007 *Opt. Express* **15** 6036–43
[90] Flöter B, Jurani P, Großmann P, Kapitzki S, Keitel B, Mann K, Plönjes E, Schäfer B and Tiedtke K 2011 *Nucl. Instrum. Methods Phys. Res. A* **635** S108–12
[91] Mey T, Schäfer B, Mann K, Keitel B, Kreis S, Kuhlmann M, Plönjes E and Tiedtke K 2013 *Proc. SPIE* **8778** 87780H
[92] Schäfer B, Mey T, Mann K, Keitel B, Kreis S, Kuhlmann M, Plönjes E and Tiedtke K 2013 *Proc. SPIE* **8778** 877810
[93] Ayvazyan V *et al* 2003 *Nucl. Instrum. Methods Phys. Res. A* **507** 368–72
[94] Juranic P N, Martins M, Viefhaus J, Bonfigt S, Jahn L, Ilchen M, Klumpp S and Tiedtke K 2009 *J. Instrum.* **4** P09011
[95] Levenberg K 1944 *Q. Appl. Math.* **2** 164–8
[96] Marquardt D W 1963 *J. Soc. Ind. Appl. Math.* **11** 431–41
[97] GNU is not Unix 2015 GNU Scientific Library online: https://gnu.org/software/gsl
[98] Bebb H B and Gold A 1966 *Phys. Rev.* **143** 1–24
[99] Agostini P, Barjot G, Bonnal J, Mainfray G, Manus C and Morellec J 1968 *IEEE J. Quantum Electron.* **4** 667–9
[100] Kramida A, Ralchenko Y, Reader J and Team N A Nist atomic spectra database online: http://physics.nist.gov/asd
[101] Amusia M Y, Dolmatov V K and Romanenko V M 1988 *J. Phys. B: At. Mol. Opt. Phys.* **21** L151
[102] Cowan R D 1981 *The Theory of Atomic Structure and Spectra Los Alamos Series in Basic and Applied Sciences* (Berkeley, CA: University of California Press)
[103] Hilborn R C 1982 *Am. J. Phys.* **50** 982–6